Layer-by-Layer Construction of Ultrathin Hybrid Films with Proteins and Clay Minerals

ARTICLE *in* THE JOURNAL OF PHYSICAL CHEMISTRY C · AUGUST 2007

Impact Factor: 4.77 · DOI: 10.1021/jp0722861

Layer-by-Layer Construction of Ultrathin Hybrid Films with Proteins and Clay Minerals

Tamás Szabó,*,†,‡ Márta Szekeres,‡ Imre Dékány,‡,§ Carine Jackers,|| Steven De Feyter,|| Cliff T. Johnston,⊥ and Robert A. Schoonheydt*,†

Centrum voor Oppervlaktechemie en Katalyse, Kasteelpark Arenberg 23, and Afdeling Moleculaire en Nanomaterialen, Departement Chemie, and Institute for Nanoscale Physics and Chemistry, Celestijnenlaan 200-F, Katholieke Universiteit Leuven, B-3001 Leuven, Belgium, Department of Colloid Chemistry and Nanostructured Materials Research Group of the Hungarian Academy of Sciences, University of Szeged, Aradi vértanúk tere 1, H-6720 Szeged, Hungary, and Crop, Soil and Environmental Sciences and Birck Nanotechnology Center, Purdue University, 915 West State Street, West Lafayette, Indiana 47907-2054

Received: March 22, 2007; In Final Form: June 20, 2007

Mono- and multilayered clay mineral−protein films were constructed with the layer-by-layer deposition technique. The clay mineral saponite and three proteins (protamine, lysozyme, and papain) were tested. Multilayers with up to 15−15 alternating layers of saponite and protein were built up on glass, quartz, and ZnSe. In some cases these supports were primed with the poly(diallyldimethylammonium) cation before clay/protein deposition. The deposition process can be followed by UV and attenuated total reflectance Fourier transform infrared (ATR-FTIR) spectroscopy and by atomic force microscopy (AFM). X-ray diffraction (XRD) patterns confirm the regular ordering of the layers. The "average" protein layer has the thickness of single molecules. The thickness of the "average" saponite layer is proportional to the positive charge density of the protein and varies between 0.6 and 3 elementary saponite sheets. The layers of protamine and lysozyme are stable. However, a small amount of papain is lost upon deposition of the subsequent saponite layer. H−D exchange of proteins in the films is fast and reversible.

Introduction

Layer-by-layer (LbL) assembly of multilayered films is now a well-established procedure for the construction of functional nanofilms.[1−3] The method is based on the alternate deposition of layers of oppositely charged polyelectrolytes, suggesting that electrostatic interaction is the main driving force for the construction of ultrathin films. Charged nanosized particles can also be used to alternate with layers of oppositely charged polyelectrolytes.[4−8] Smectites or swelling clays are well suited for that purpose. They are negatively charged due to isomorphous substitution. This charge is neutralized by exchangeable cations in the interlamellar space. The clay minerals are thus hydrophilic and take up water in the intergallery space. In air-dried samples there is a monolayer of water; in water they swell and fall apart into elementary sheets of 0.96 nm. Thus mono- and multilayers of single clay sheets and cationic polyelectrolytes such as PD [poly(diallyldimethylammonium chloride)] can be constructed.[9−13] The elementary clay platelets not only impart mechanical strength to the film but also organize molecules at their surface in specific configurations, depending on the charge density of the clay and the size, shape, and charge of the molecules.[14] Thus ultrathin clay films have been produced by the LbL technique with water sensing,[15] magnetic,[16] antimicrobial,[17] and nonlinear optical properties.[18]

Proteins can in principle also be used in combination with smectite clays to produce ultrathin films for biosensing and biocatalysis.[19−21] Lamellar smectite particles are especially feasible for this purpose due to their biocompatible surface combined with their unique intercalation properties,[22−24] high surface area, and short-range templating effect.[25,26] Moreover, the silicate sheets bearing permanent negative charges facilitate the adsorption of positively charged enzymes[27,28] or enzyme-mimicking metal complexes.[29,30] Such electrostatic interactions can be exploited for the construction of multilayered, bioactive ultrathin films as well. However, the interaction of proteins with smectite particles is complex and involves protein−clay surface, protein−water, protein−protein, and clay surface−water interactions.[31] For example, the maximum amount of bovine serum albumin (BSA) sorption was achieved around the isoelectric point (IEP) of BSA, suggesting that not only the electrostatic interaction plays a role.[32] Nevertheless, proteins are usually immobilized by charged polymers acting as electrostatic "sticking materials".[33,34] Biorelated application of proteins in such systems may suffer from the drawbacks of polyion-induced aggregation and/or denaturation. Furthermore, the targeted substrate species of the enzyme reaction may have limited accessibility to the enzyme molecules wrapped in the polymer matrix. Colloids other than flexible macromolecules for film preparation are therefore highly demanded. Lvov et al.[34] showed that clay sheets underwent self-assembly with positively charged myoglobin or lysozyme on quartz or silicon surfaces. However, they found that only one bilayer (clay/protein) could be formed unless polyelectrolytes were applied to keep together the neighboring species.

The protein species chosen for our investigations is papain, which is a powerful proteolytic (peptide-bond cleaving) enzyme

* Authors to whom correspondence should be addressed: e-mail Tamas.Szabo@biw.kuleuven.be or sztamas@chem.u-szeged.hu (T.S.), Robert.Schoonheydt@biw.kuleuven.be (R.A.S.).

† Centrum voor Oppervlaktechemie en Katalyse, K.U. Leuven.

‡ Department of Colloid Chemistry, University of Szeged.

§ Nanostructured Materials Research Group of the Hungarian Academy of Sciences, University of Szeged.

|| Afdeling Moleculaire en Nanomaterialen and INPAC, K.U. Leuven.

⊥ Purdue University.

10.1021/jp0722861 CCC: $37.00
Published on Web 08/04/2007

derived from the papaya fruit (*Carica papaya* L.). Papain is primarily used in food processing technologies as a meat tenderizer and for chill-proofing of beer.[35] It has applications in the paper and adhesive industries as well as in sewage disposal. In medicine, its digestive property is also exploited for acceleration of wound healing, soothing of stomach, and damaging the cuticles of parasitic nematodes.[36] In spite of its primary importance in biotechnology, there are no studies for the incorporation of papain into biofunctional, self-assembled nanofilms. Here we report on the successful deposition of papain/clay multilayers by self-assembly. The properties and build-up of papain films are compared with those of clay films of protamine (a small, arginine-rich polypeptide used in DNA binding assays) and lysozyme (a glycosidase enzyme with antibacterial properties).

Focusing especially on the construction of the above clay−protein films, we show that (1) multilayered films can be deposited on different substrates (glass, quartz, ZnSe); (2) the first layer does not need to be a polyelectrolyte, as often reported in the literature; (3) layer-by-layer construction can be followed by different spectroscopic techniques; and (4) build-up of the layers of smectite particles and of protein molecules can be monitored separately.

Experimental Section

Materials. Papain (from papaya latex; $M_w = 23\,400$; E.C. 3.4.22.2), lysozyme (from chicken egg white; $M_w = 14\,300$; E.C. 3.2.1.17), and the histone-free sulfate salt of protamine (from herring, grade III; $M_w = 4500$) were obtained from Sigma and used without further purification. Protamine, in a strict sense, is a polypeptide without enzyme activity, but it will be referred to, together with the other two biomolecules, as "protein". A natural saponite specimen (purchased from the Source Clays Repository of the Clay Minerals Society) was used as the layer silicate host for the protein immobilization. The crude clay was first Na^+-saturated by repeated (three times) exchange with 1 M NaCl solutions, followed by dialysis with water until Cl^--free (tested by $AgNO_3$). The sample was fractionated by centrifugation and the $d < 500$ nm fraction was selected for the self-assembly. As a cationic polymer, poly(diallyldimethylammonium chloride) (PD) with medium molecular weight [$M_w = (2-3) \times 10^5$] was purchased from Aldrich and was used as a 20 wt % aqueous solution. NaOH (Riedel de Haën) and HNO_3 (Fluka) were used for pH setting, while D_2O (99,8 at. % D, Acros Organics) was purchased for deuteration experiments. All aqueous solutions and dispersions were prepared in distilled water filtered with a Millipore Milli-Q system (MQ water).

Preparation of Biomolecular LbL Films. Multilayered films were deposited on glass and quartz substrates and on ZnSe crystal by the layer-by-layer self-assembly method. Quartz slides were used for UV−vis and X-ray diffraction (XRD) measurements. Thin glass (Menzel Gläser, 24 × 61 mm, Fischer Sci. Ltd) platelets were supports for atomic force microscopy (AFM) investigations, and the ZnSe crystal served as the internal reflection element (IRE) for attenuated total reflectance Fourier transform infrared (ATR-FTIR) spectroscopy. The latter was cleaned by polishing with an aqueous slurry of cerium oxide. Quartz and glass slides were cleaned by sonication in a detergent solution. Then they were put in chromic acid for at least 20 min in order to remove adsorbed surfactants. The substrates were then extensively rinsed with MQ water, dried under a stream of dust-free nitrogen, and immediately used for the self-assembly procedure.

The papain multilayers were built up through the following steps: (1) Substrates were immersed in a 0.1% solution of the positively charged PD molecules. (2) Slides were then immediately rinsed with copious amounts of MQ water and dried under a stream of nitrogen at room temperature. (3) Substrates with the adsorbed PD monolayer were submerged into the saponite suspension (0.5%), followed by washing and drying. (4) Slides were dipped into papain solution (0.2%), always freshly prepared to avoid the unwanted effects of potential autoproteolytic degradation. (5) PD-coated platelets, containing now one hybrid saponite/protein bilayer, were washed again with MQ water and dried. (6) Operation steps 3−5 were successively repeated (up to 14 times). The buildup protocol was periodically interrupted for UV−vis or ATR measurements. Deposition times were either 5 min (when the films were deposited on quartz for UV−vis measurements) or 30 min (for films deposited on glass for AFM or ZnSe for ATR spectroscopy).

This procedure afforded a composite biomolecular film that consisted of 15 layers of saponite sheets alternating with 15 layers of papain molecules. They will be referred to as S-PD-$(Sa/PA)_{15}$. (S = substrate, Sa = saponite, PA = papain; the sequence listed is the sequence of deposition). In some cases the papain/clay bilayers were deposited directly on the bare supports. For such films the first two steps were omitted and the dipping started with step 4. The sequence of deposition is then papain/saponite (PA/Sa). Self-assembly was studied at two different pH values (4 and 8). These pHs are close to the inherent pH of the 0.2% papain solution (3.8−4.2) and that of the 0.5% saponite suspension (8−8.3). Accurate pH setting (to pH unit ±0.1 near the desired value) with NaOH and HNO_3 solutions was performed, if necessary. Other types of assemblies were prepared from lysozyme (LZ/Sa) and protamine (PR/Sa) by an identical dipping/washing protocol, although deposition of the PD support layer was omitted for these proteins.

The self-assembly of these protein/clay systems is quite rapid with typical deposition times of 5 min. It was also found that sonication of the clay suspension before deposition gave films of better homogeneity.

Characterization Techniques. UV−visible spectra of the protein solutions, clay suspensions (reference, water), and self-assembled nanofilms (reference, bare light path) were recorded on a Perkin-Elmer Lambda 12 double-beam spectrophotometer. The spectra of the quartz slides were recorded separately and substracted from the spectra of the quartz slides carrying the films.

X-ray diffraction measurements were performed on a Philips PW 1830 diffractometer operating with a Cu anode (40 kV voltage, 30 mA cathodic current). Cu Kβ radiation was absorbed by a Ni filter; $\lambda_{Cu\ K\alpha} = 1.542$ nm.

ATR-FTIR spectra were collected on a Bruker IFS 66v/S spectrometer. Films were deposited on ZnSe 45° trapezoidal-shaped crystals (SPT-Harrick, 50 × 20 × 2 mm) with 25 internal reflections and were measured in an ATR cell. The crystals were always polished before deposition. For deuteration, the crystals covered with the films were immersed in D_2O for 2 h and then transferred rapidly (in less than 15 s) to the measurement cell, which was immediately evacuated to avoid H−D back exchange. A total of 128 scans were accumulated for each spectrum. The spectral resolution was 2 cm^{-1}. The 4000−2500 cm^{-1} region of the spectra were smoothed with a 15-point Savitzky−Golay function.

Atomic force microscopy (AFM) was used to investigate the mono- and multilayer surface topography. AFM measurements were performed with a Discoverer TMX2010 AFM system (ThermoMicroscopes, San Francisco, CA) operating in non-

contact mode with MPP-11120−Tap300Metrology probes (ThermoMicroscopes, San Francisco, CA) with a spring constant of 400 N/m and a resonance frequency of around 270−280 kHz. The topographs were processed (background substraction with standard "roll ball" algorithm and subsequent second-order plane leveling) and analyzed (line and area analysis) by the TopoMetrix SPMLab NT 5.0 software.

Definition of AFM Parameters: *Average height level* ($\bar{Z}$) is the arithmetic mean, defined as the sum of all height values divided by the number of data points:

$$\bar{Z} = \frac{1}{N}\sum_{i=1}^{N} Z_i \tag{1}$$

Root-mean-square roughness (R_{ms}) is the square root of the mean value of the squares of the distance of the points from the image mean value:

$$R_{ms} = \sqrt{\frac{1}{N}\sum_{i=1}^{N}\langle Z_i - \bar{Z}\rangle^2} \tag{2}$$

Maximum peak-to-valley range (ζ) is the difference between the highest and lowest points of the whole image area:

$$\zeta = Z_{max} - Z_{min} \tag{3}$$

Results

Multilayer Formation As Measured by UV−Vis Spectroscopy. In the first set of experiments, we aimed at the establishment of assembly conditions that afford papain/clay nanofilms without the application of the cationic polymer (PD). The layers were built on quartz slides and the process was monitored by recording the UV−vis spectra in the 190−500 nm range. Besides the conventional deposition series (i.e., PD/Sa/PD/PA), we found from the regular increase of the absorbance that it was possible to obtain PD-(Sa/PA)$_n$ films. Moreover, to our surprise, complete omission of the polymer also proved to be viable, and the as-compiled, slightly opaque (PA/Sa)$_n$ assemblies seemed to be homogeneous by visual observation. Besides papain, protamine and lysozyme could also directly form multilayers with saponite [(PR/Sa)$_n$ and (LZ/Sa)$_n$]. Thus, the linking ability of proteins seems to be quite general. This phenomenon is not widely realized and only a very few examples of protein films without polyelectrolyte "glue" are published.[37]

Figure 1 shows the UV−vis spectra of the (PA/Sa)$_{15}$, (PR/Sa)$_{15}$, (LZ/Sa)$_{15}$, and (PD/Sa)$_{15}$ films. The hybrid protein/saponite multilayers have a definite absorbance maximum at 194 nm ($\pi^* \leftarrow \pi$ transition) with a shoulder at ca. 230 nm (symmetry-forbidden $\pi^* \leftarrow$ n transition) characteristic of peptide bonds.[38] Papain and lysozyme have a weak additional band around 260 nm originating from the aromatic amino acid residues (tyrosine, tryptophan, and phenylalanine). Protamine does not have this weak absorbance, as it lacks these amino acids.

The absorbance of the (PD/Sa)$_n$ films is weakly increasing from the visible into the UV range. Its increase at each wavelength is nearly proportional to the number of layers. Since PD is fully transparent, the spectra of the (PD/Sa)$_n$ multilayers are due to the scattering and absorbance of the saponite particles in the films. Thus, it is possible to subtract the PD/saponite ("clay") spectra from those of the protein/clay systems to obtain the UV−vis spectra of the protein phase in the multilayers.

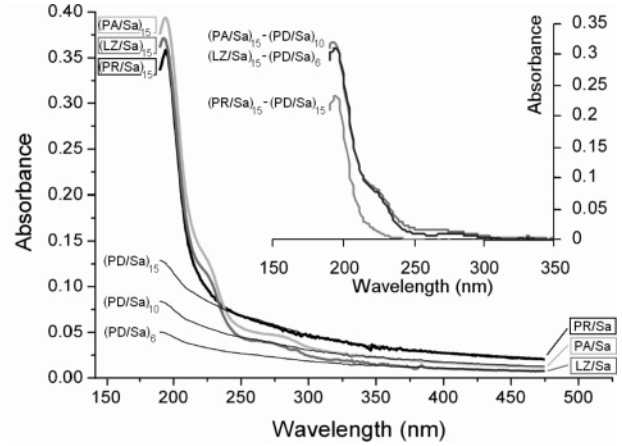

Figure 1. UV−vis spectra of (PA/Sa)$_{15}$, (LZ/Sa)$_{15}$, and (PR/Sa)$_{15}$ multilayers deposited at pH 8, together with those of corresponding (PD/Sa)$_n$ assemblies. (Inset) Difference spectra of "pure protein" films.

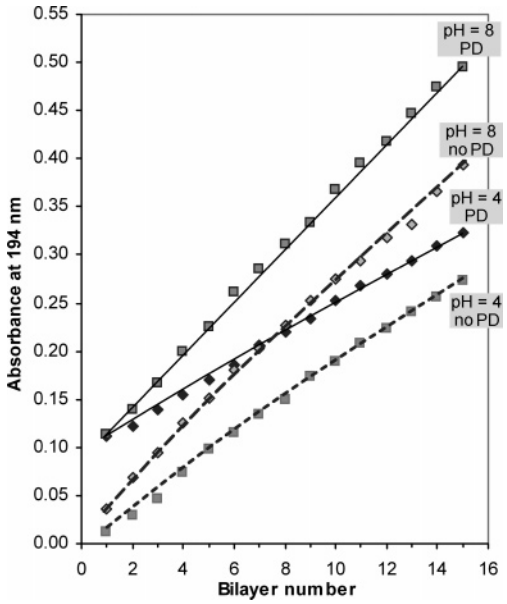

Figure 2. Absorbances (at 194 nm) of PD-(Sa/PA)$_n$ and (PA/Sa)$_n$ multilayer films ($n = 1-15$) deposited on quartz surfaces at pH 4 and 8.

These spectra are shown in the inset of Figure 1. These spectra are the same as those of the proteins (measured, not shown). One remarks that the number of layers of (PD/Sa)$_n$ used for substraction is different for each protein. This is because we have chosen (PD/Sa)$_n$ absorbance lines in the 320−500 nm region, which fall together with those of the protein films with 15 bilayers.

Layer-by-Layer Construction. The absorbance at 194 nm (not corrected for light scattering by saponite particles) is plotted versus the number of bilayers n in Figure 2 for PD-(Sa/PA)$_n$ and (PA/Sa)$_n$ films. For the system PD-(Sa/PA)$_n$, one observes a jump of the absorbance for $n = 1$ from 0 to 0.1, followed by a linear increase with n. For PA the slopes of the lines are 0.0276 for deposition at pH 8 and 0.0154 for deposition at pH 4. It means that for $n > 1$ the amount of saponite and papain deposited in one layer is, on average, the same for all layers up to $n = 15$. The jump in absorbance for the first bilayer indicates that large amounts of saponite and papain are deposited on PD. For the (PA/Sa)$_n$ multilayers, the jump in absorbance at $n = 1$ is absent. The absorbance increases almost linearly with layer number but a slight bending is observed around $n = 4-6$.

TABLE 1: Amounts, Packing Densities,and Surface Areas Per Molecule in Deposited Protein Layers[a]

sample	n^S (ng/mm^2)	Θ (nm^{-2})	Ω (nm^2)	ω (nm^2)
1st bilayer of PD-(Sa/PA), pH 8	14.7	0.378	2.6	11.9
2nd−15th bilayers of PD-(Sa/PA), pH 8	2.4	0.073	13.1	11.9
1st bilayer of PD-(Sa/PA), pH 4	14.7	0.372	2.7	11.9
2nd−15th bilayers of PD-(Sa/PA), pH 4	1.6	0.041	24.2	11.9
$(PA/Sa)_{15}$, pH 8	2.8	0.076	13.7	11.9
$(PA/Sa)_{15}$, pH 4	2.0	0.050	19.9	11.9
$(LZ/Sa)_{15}$	1.4	0.059	17.0	10.6
$(PR/Sa)_{15}$	1.1	0.145	6.9	6.3

[a] n^S, amount; Θ, packing density; Ω, calculated surface area per molecule; ω, theoretical surface area per molecules

These absorbances at 194 nm, after substraction of the contribution of the saponite particles (see Appendix), were used for calculation of the amount (n^S), packing density (Θ), and average surface area per molecule (Ω) of deposited protein molecules (Table 1). These latter are compared with theoretical surface areas (ω), which were obtained under the assumption of spherical molecules with equivalent diameters of 3.7, 3.5, and 2.7 nm for PA,[39] LZ,[40] and PR,[40] respectively, and hexagonal close packing. We find good agreement with the case of PR and PA at pH 8 [for the PD-$(Sa/PA)_n$ films, this applies only to the secondthrough 15th bilayers]. For PA at pH 4 and LZ, the area per molecule in the multilayered films exceeds the area of hexagonally close packed spheres. This indicates less than monolayer coverage. A possible reason is the high positive charges resulting in protein−protein repulsion. However, this is not the only reason, as protamine is the smallest molecule and it carries the highest charge.

As mentioned above, a distinctive characteristic of the PD-$(Sa/PA)_n$ films is the higher amount of protein deposited in the first bilayer. This is also quantitatively reflected in the fact that their respective Ω values are 5−10 times higher than those found in the absence of PD. Thus, it must be concluded, similarly to the previously reported glucose oxidase/poly-(ethylenimine) system,[34] that the protein molecules adjacent to the polyelectrolyte form aggregates, resulting in apparent multilayer formation. This polyion-induced aggregation seems to be quite general for protein/polyelectrolyte alternating multilayers.[34] Such an agglomeration is, though, not favored between the clay lamellae, and the film growth does not exceed monolayer thickness.

When the absorbance at 194 nm, measured after each deposition of saponite and after each deposition of proteins, is plotted versus the bilayer number, Figure 3 is obtained. In the case of $(LZ/Sa)_n$ and $(PR/Sa)_n$ (the latter not shown), the absorbance increases after each deposition of lysozyme and remains constant (within experimental accuracy) after the subsequent deposition of saponite particles. This is in agreement with Figure 1, which shows that the absorbance of saponite (due to scattering) is small when compared to that of the proteins. It is also remarkable that the build-up functions of the $(LZ/Sa)_n$ and $(PR/Sa)_n$ films determined at pH 8 fall together with those deposited at pH 4 (the latter are not shown).

For papain, a similar jump in absorbance at 194 nm is observed after each deposition of papain. However, it decreases slightly after the subsequent deposition of saponite. This clearly indicates loss of papain. It might indicate that some papain−clay complexes are washed away. The question is then why it does not occur in the case of lysozyme or protamine. Another possibility is that a small part of the papain decomposes upon contact with saponite particles.

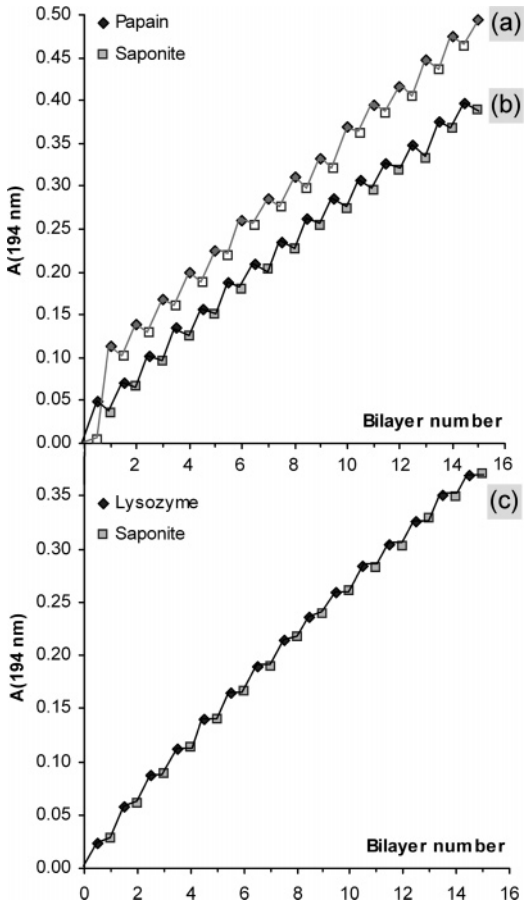

Figure 3. Absorbances (at 194 nm) of (a) PD-$(Sa/PA)_n$, (b) $(PA/Sa)_n$, and (c) $(LZ/Sa)_n$ hybrid multilayers ($n = 1-15$) deposited on quartz at pH 8. For each film, diamonds and squares represent the absorbances measured after deposition of protein molecules and of saponite particles, respectively.

ATR-FTIR Spectroscopy. Figure 4 shows the ATR spectrum of $(LZ/Sa)_3/LZ$ (that is, a film consisting of three saponite layers sandwiched between four protein layers) deposited at pH 4. The spectra of the other two protein films are not shown as they exhibit the same spectral features. Three distinct spectral regions can be distinguished. The first is located between 3600 and 2800 cm^{-1}. It includes the C−H stretching vibrations in the 2800−3000 cm^{-1} region, the amide A band of lysozyme around 3300 cm^{-1} (related to N−H stretching),[41] and the stretching vibration of the structural OH groups of saponite at 3640 cm^{-1} (not clearly resolved). A set of bands between 1750 and 1450 cm^{-1} follows that is characteristic of the amide groups of the protein backbone. The so-called amide I band appears at around 1650 cm^{-1} and is mainly due to the C═O stretch, while the amide II band at 1550 cm^{-1} characterizes mainly the N−H bending.[42] Finally, the 1000 and 1064 cm^{-1} peaks correspond to the in-plane and out-of plane ν(Si−O) modes of saponite.[43]

The inset of Figure 4 shows the FTIR spectra of the proteins. They show peaks in the same spectral window as given above with the exception of the 1200−800 cm^{-1} region, where papain has several bands with the most intense at 1024 cm^{-1}, protamine has a band at 1100 cm^{-1}, and lysozyme does not show any adsorption band. These bands are indicative of the presence of anions in the proteins: phosphate in papain and sulfate in protamine.

Proteins in the Films. Since the infrared absorption bands of the individual components (i.e., clay and protein) are

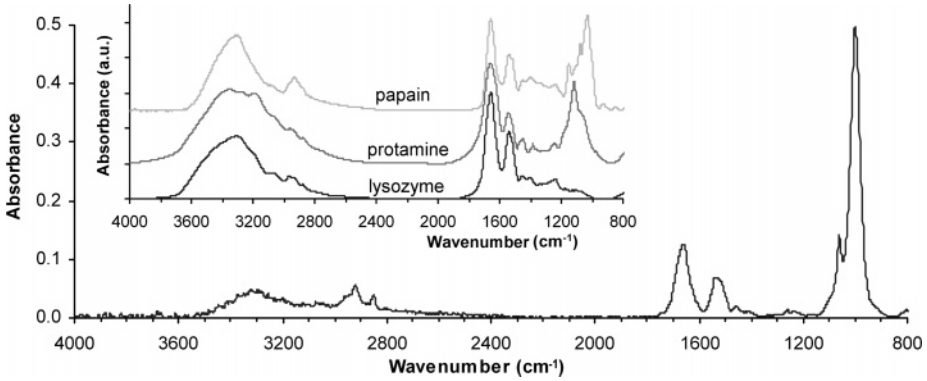

Figure 4. ATR spectrum of $(LZ/Sa)_3$/LZ film. (Inset) FTIR spectra of the three proteins.

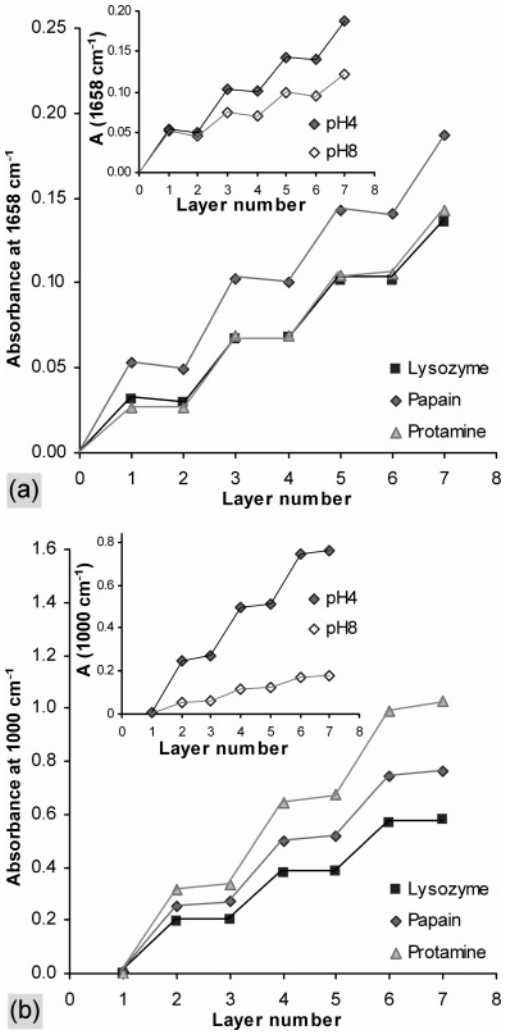

Figure 5. IR absorbance of (a) amide I band (at 1658 cm^{-1}) and (b) in-plane Si−O band (at 1000 cm^{-1}) of the protein/saponite assemblies deposited on ZnSe crystal at pH 4 as a function of the number of individual layers. (Insets) Build-up functions of papain films deposited at pH 4 and 8.

completely resolved, it is possible to monitor the build-up of the protein and saponite layers separately. Figure 5a gives the absorbance of the amide I band (1658 cm^{-1}) of the three protein/clay films deposited at pH 4 with the layer numbers. The $(LZ/Sa)_n$ and $(PR/Sa)_n$ assemblies show identical stepwise build-up patterns after each deposition of a protein layer (odd layer numbers). The absorbance increases by ca. 0.03 absorbance unit and is independent of the layer number. There is no change in absorption upon deposition of a saponite layer, indicating that the amount of deposited protein is unperturbed by the saponite deposition process. The absorbances of $(PA/Sa)_n$ films deposited at pH 4 at 1658 cm^{-1} are higher than those of the $(LZ/Sa)_n$ and $(PR/ Sa)_n$ films. The average increase in absorbance is 0.05, independent of the layer number. There is also a clear pH dependence: the average absorbance increase per deposited papain layer is 0.025 at pH 8. Interestingly, the absorbance increase for the first papain layer is 0.05, identical for both pH values. Finally, after deposition of a saponite layer, the 1658 cm^{-1} band decreases slightly. This is indicative of a small loss of papain upon adsorption and washing of the saponite layer.

Clay in the Films. The absorbance of the clay band (at 1000 cm^{-1}) versus layer number of the films is plotted in Figure 5b. Now, the absorbance increases after deposition of clay layers (even layer numbers). The average increase of the absorbance per deposited saponite layer is 0.20, 0.25, 0.32, and 0.06 for $(LZ/Sa)_n$, $(PA/Sa)_n$, $(PR/Sa)_n$, and $(PA/SA)_n$ at pH 8, respectively. It is apparent, thus, that the protamine films contain higher amount of clays as compared to the other two proteins. This agrees well with the observed differences in the 300−500 nm region of the UV−vis spectra related to the clay scattering of the films (Figure 1). After the deposition of proteins (odd layer numbers), the absorbance at 1000 cm^{-1} remained constant. There was no decrease due to loss of clay. There was no increase either, although there are complex strong bands centered at 1100 and 1024 cm^{-1} in pristine papain and protamine powders (inset, Figure 4). These bands are attributed to charge-neutralizing anions such as SO_4^{2-} or phosphate present in the solid.[44] The spectra of the protein monolayers (not shown) on the substrate (without saponite) lack these bands as well. This suggests that phosphate and sulfate anions are absent in the films. Therefore, the absorbance of the Si−O band at 1000 cm^{-1} can be reliably used as a measure of the clay content in such thin films. In a previous paper we estimated the absorbance of the 1000 cm^{-1} Si−O band due to a monolayer of saponite sheets to be 0.103 au.[43] Thus, the absorbances of 0.2, 0.25, 0.32, and 0.06 correspond with layers consisting of 2, 2.5, and 3 elementary saponite sheets of 1 nm thickness for $(LZ/Sa)_n$, $(PA/Sa)_n$ and $(PR/Sa)_n$ films at pH 4 and only 0.6 sheet for $(PA/Sa)_n$ at pH 8, respectively.

Water in the Films. The 4000−2500 cm^{-1} region of the ATR spectra of $(PR/Sa)_n$ films is shown in Figure 6. The sharp band at 3680 cm^{-1} is the OH stretch of the structural hydroxyl groups of saponite.[43] The intensity of this peak increases with the number of deposited clay layers. On the other hand, the absorbance of the broad band between 3500 and 2800 cm^{-1} increases with the number of protamine layers. There is no visible absorption between 3680 and 3500 cm^{-1}. This is indicative of the absence of detectable amount of water. Similar observations were made for $(PA/Sa)_n$ and $(LZ/Sa)_n$.

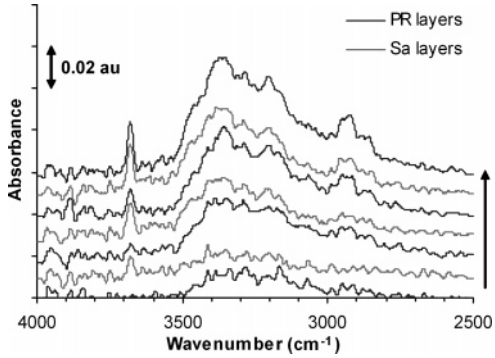

Figure 6. ATR spectra (4000−2500 cm^{-1} region) of $(PR/Sa)_n$ films up to 7 layers ($n = 3.5$). For clarity, spectra are offset by 0.01 absorbance unit.

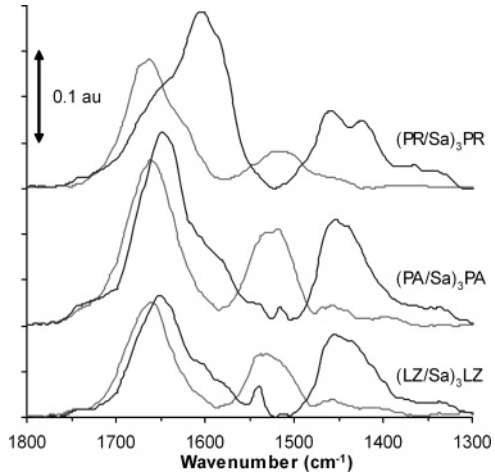

Figure 7. Amide I and II region of the IR spectra of $(LZ/Sa)_3LZ$, $(PA/Sa)_3PA$, and $(PR/Sa)_3PR$ films deposited at pH 4 before (gray lines) and after (black lines) deuteration for 2 h.

Deuteration. Some information on the conformation of the adsorbed protein layers is obtained by deuteration experiments. The 1300−1800 cm^{-1} range of the spectra of the as-prepared and deuterium-exchanged protein films are compared in Figure 7. For the three proteins, the amide II band shifts from about 1520 to 1450 cm^{-1} upon deuteration (the latter wavenumber is also measured for the proteins dissolved in D_2O). The shift is in agreement with expectation, as the amide II band is mainly composed of N−H bending vibrations. Within the time span of the deuteration experiment (2 h), the amide II band of protamine is completely deuterated, while for papain and lysozyme, small residual bands remain at 1512 and 1539 cm^{-1}, respectively. This indicates incomplete deuteration. Clearly, papain and lysozyme have hydrophobic regions that are difficult to deuterate. On the other hand, protamine, with its small molecular weight and a loose helix structure,[45] can be rapidly and fully deuterated. In all cases the H−D exchange is reversible; replacing D_2O by H_2O gives the original spectra again. The amide I band of papain and lysozyme shifts by 10−15 cm^{-1} toward lower wavenumbers upon D_2O exchange. The reason for this is that there is some coupling of the C═O with N−H bending.[46] The shift of the amide I band of protamine is much more pronounced (ca. 60 cm^{-1}). This is due to the presence of guanidinium ions in arginine, which constitutes ca. 80% of the residues of protamine; both the $\delta(NH_3^+)$[47] and the ν(C−N) vibrations of guanidinium ions contribute to the amide I band.[48] These vibrations are obviously more affected by the D exchange than the amide I band, with a primary contribution of the C═O vibrations.

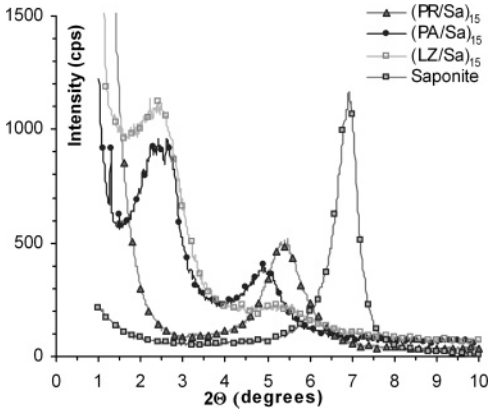

Figure 8. XRD patterns of freeze-dried saponite and $(LZ/Sa)_{15}$, $(PR/Sa)_{15}$, and $(PA/Sa)_{15}$ nanofilms deposited at pH 8 on quartz.

TABLE 2: Basal Distances of Pristine Saponite and Different Protein/Clay Nanofilms

sample	d_{001} (nm)	d_{002} (nm)
freeze-dried saponite	1.28	
$(PD/Sa)_{15}$	1.47	
$(PR/Sa)_{15}$	1.64	
$(LZ/Sa)_{15}$	3.56	1.64
$(PA/Sa)_{15}$, pH 8	3.53	1.77
$(PA/Sa)_{15}$, pH 4	3.20	1.64
PD-$(Sa/PA)_{15}$, pH 8	3.53	1.77
PD-$(Sa/PA)_{15}$, pH 4	3.20	1.64

X-ray Diffraction. The diffraction patterns of the pristine clay and of the self-assembled protein/clay nanofilms consisting of 15 bilayers are presented in Figure 8, while the corresponding basal spacings are given in Table 2. The (001) reflection of saponite appears at $2\Theta = 7.0°$, which refers to a repeat distance of 1.28 nm. This is typical for air-dried smectite clays containing Na^+ and a monolayer of water molecules in the interlamellar space. The basal distance of 1.45 nm found for the $(PD/Sa)_{15}$ nanofilm is practically identical with those reported for various PD/clay systems.[11,12,15] The 1.45 nm spacing could be ascribed either to intercalation of PD or to a clay hydrate with two layers of water in the interlamellar space. In view of the alternate deposition of saponite layers and PD layers we favor the first explanation, which is also supported by ATR spectroscopy, revealing that there are no detectable amounts of water in the films. $(LZ/Sa)_{15}$ and $(PA/Sa)_{15}$ assemblies have d_{001} spacings around 3.5 nm, which corresponds to an intergallery height of 2.5−2.6 nm. This is somewhat smaller than the crystallographic sizes of papain (3.7 × 3.7 × 5 nm)[39] and lysozyme (3 × 3 × 4.6 nm).[49] Interestingly, the same basal spacing was found by Zhou et al.[19] for a clay film assembled with hemoglobin, which is a much larger molecule (5 × 5.5 × 6.5 nm).[50] The authors assumed that hemoglobin was partly intercalated between disordered clay layers in the films. In the case of $(PA/Sa)_{15}$ and $(LZ/Sa)_{15}$ films, however, the gallery height still seems large enough to accommodate the papain and lysozyme molecule. The protein-saponite interaction and the lack of detectable amounts of water in the films are the probable reasons for the shrinkage of the protein molecules.

The most prominent feature of the XRD patterns of $(LZ/Sa)_{15}$ and $(PA/Sa)_{15}$ films is the marked presence of a well-developed second-order reflection at $2\Theta = 5°$ and 5.3° for films deposited at pH 8 and 4, respectively. The appearance of a (002) diffraction peak reveals a well-defined layer-by-layer order. This is especially remarkable because for single polyelectrolyte/clay multilayers such a highly ordered structure is not observed.[11,12] A similar degree of long-range ordering was reported only for

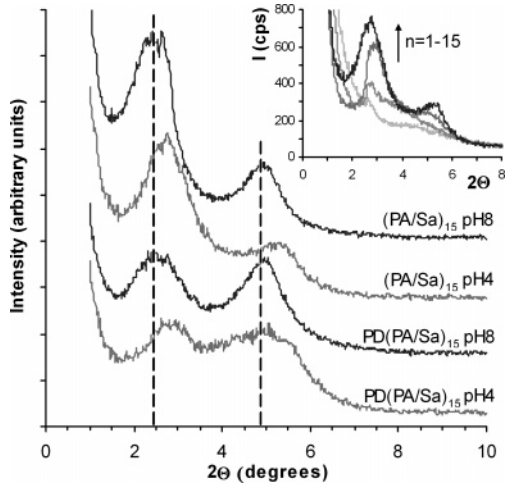

Figure 9. XRD patterns of $(PA/Sa)_{15}$ and PD-$(Sa/PA)_{15}$ biofilms deposited at pH 4 and 8. (Inset) X-ray diffractograms of $(PA/Sa)_n$ films deposited at pH 4; $n = 1$, 2, 5, and 15.

montmorillonite assembled with stiff molecules such as sexithiophene combined with two short cationic alkyl chains.[51]

Figure 9 compares the diffractograms of PD-$(Sa/PA)_{15}$ and $(PA/Sa)_{15}$ biofilms deposited at pH4 and 8. The reflections of $(PA/Sa)_{15}$ films (at both pHs) follow a regular, nearly exponentially decaying (00*l*) series, indicating the dominance of a uniform, single crystallographic phase consisting of the "sandwich-like" protein/clay structure when the layers are directly deposited on the surface of the support. On the other hand, the (002) reflections of the PD-$(Sa/PA)_{15}$ films are broader and are almost of the same intensity as the (001) diffraction peaks, suggesting that the peak centered at $2\Theta = 5°$ is not only of pure (002) character. This points to a less ordered structure that forms when the protein/clay multilayers are assembled on polyelectrolyte-coated supports. Finally, the basal distances of the films are pH-dependent. At pH 8 the interplanar spacings are slightly but clearly higher than those of the films deposited at pH 4. The explanation for this difference is not straightforward; many effects may influence the size of the protein molecules confined in the interlamellar space, including their charge, hydration, and conformation states.

Atomic Force Microscopy. The topographical AFM images of papain deposited on glass at pH 4 and 8 are shown in Figure 10, panels a and b, respectively. Yellow spots are regions covered with papain molecules, while the dark, lower-lying areas correspond to bare glass. At pH 8 the diameter of these papain regions average 50−100 nm; the exact values are difficult to determine owing to ill-defined particle edges and imaging effects such as tip broadening.[52] At pH 4 the adsorption pattern involves also larger protein patches up to several hundred nanometers, which are distributed randomly across the surface. The lateral dimensions of the protein spots/islands are at least 1 order of magnitude higher than the sizes of the individual molecules. This indicates that the molecules are closer to each other than the instrumental and the image resolution, meaning that they are densely accumulated in certain regions of the glass surface. However, AFM cannot give direct information about aggregation and/or defolding upon deposition. The characteristic sizes of the protein patches in the vertical dimensions (that is, perpendicular to the substrate) are determined by standard line and area analyses. The resulting height profiles and height distribution histograms are seen in Figure 10, and AFM parameters are given in Table 3. The height of the papain islands is around 3 nm as found by several line analyses. This value

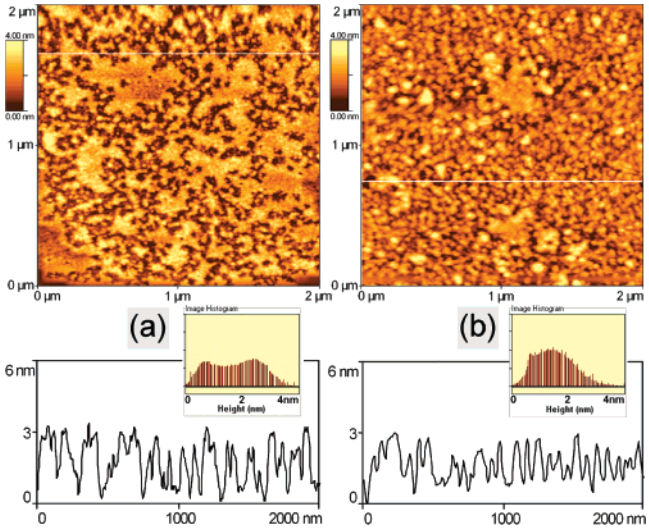

Figure 10. AFM topographical images of papain monolayers deposited at (a) pH = 4 and (b) pH = 8. Panels at the bottom represent characteristic height profiles obtained after analysis of the horizontal line marked in white in the images. (Insets) Height distribution functions of the monolayer surfaces.

TABLE 3: AFM Parameters of Bare Glass, Papain Monolayers, and Hybrid Papain/Clay Films

sample	R_{ms} (nm)	$\bar{Z}$ (nm)	ζ (nm)
glass (Menzel; Fischer GmbH)	0.28	0.40	1.3
papain monolayer deposited at pH 4	0.90	1.88	4.9
papain monolayer deposited at pH 8	0.72	1.59	4.6
$(PA/Sa)_1$ bilayer, deposited at pH 4	1.78	3.25	11.4
$(PA/Sa)_1$ bilayer, deposited at pH 8	1.36	1.76	9.1
$(PA/Sa)_5$ multilayer	4.4	8.25	20.5
PD-$(Sa/PA)_1$ triple layer	5.04	10.38	30.5

compares favorably with the reported size of the molecules (3.7 × 3.7 × 5 nm). Also, the full height range (ζ), which gives the height difference between the lowest and highest detected points of the scanned area of 2 × 2 μm, does not exceed 5 nm. It is concluded that the papain molecules form a monolayer with heights not greater than that of a single molecule. Area analysis gives also the root-mean-square roughness (R_{ms}) of the papain-modified glass surface. Although it is higher than that of the bare support, it is still very low at both pHs (0.72−0.9 nm) and is similar to that of a monolayer of myoglobin (0.85 nm),[37] a protein of nearly the same size as papain. The insets of Figure 10 give the histograms of the height distribution. This function, unlike a single line profile, is informative on the characteristic height values over the whole scanned area. The histograms are found to be bimodal at both pHs. At pH 4 the first peak with a maximum at 0.7 nm refers to the average substrate height. It is only slightly less abundant than the "protein height" at 2.4 nm. However, the substrate contribution is very low on the right-hand side histogram, referring to the protein monolayer deposited at pH 8. This means that there are very few empty spaces on the glass surface. This coincides well both with the visual observation and with the results of UV spectroscopy and the derived model calculation, which suggest that the surface coverage is higher when papain is adsorbed at pH 8.

AFM images of papain/saponite bilayers deposited on bare glass at pH 4 and 8 are compared in Figure 11a,b. Clay particles (yellow areas) are clearly discernible in both cases. They are randomly oriented and only partially cover the underlying protein monolayer. Line analysis shows that over a lateral distance of 5 μm there are 3−4 particles with heights of about 7 nm, that is, they are composed of several saponite sheets. At pH 4 the saponite particles are larger than at pH 8. Moreover,

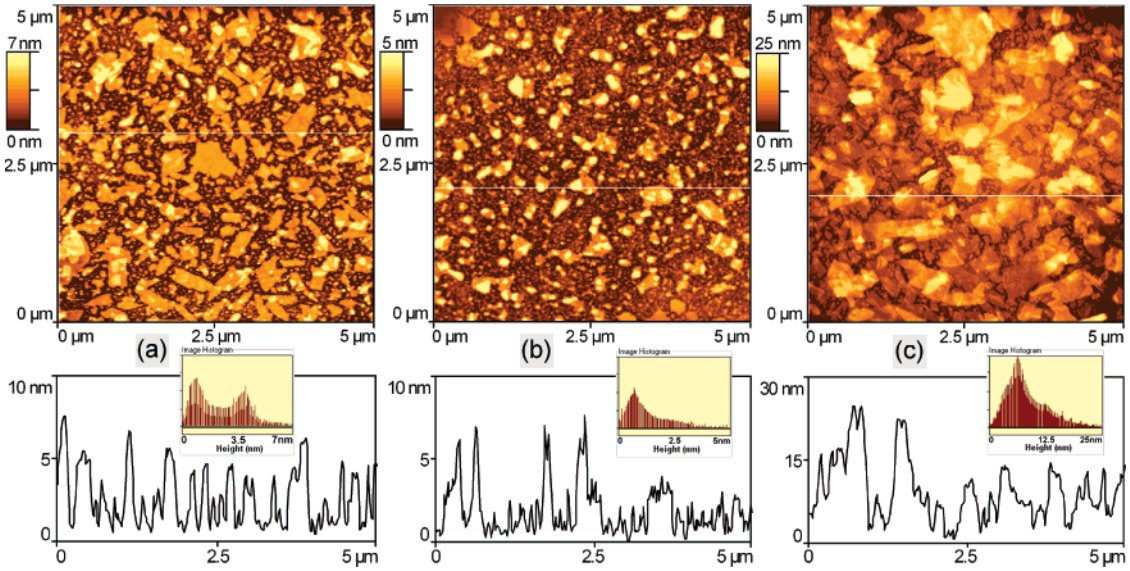

Figure 11. AFM topographical images of $(PA/Sa)_1$ bilayers, deposited at (a) pH = 4 and (b) pH = 8, and of (c) a PD-$(Sa/PA)_1$ film. Panels at the bottom represent characteristic height profiles obtained after analysis of the thin horizontal line marked in white in the images. (Insets) Height distribution functions of the films.

the surface coverage is also higher at pH 4, as can be deduced from the height histograms: the area of the "clay peak" at 4 nm (characteristic for the average height of clay layers) is only slightly lower than that of the "substrate" peak at ca. 1 nm, while the former peak has a lower contribution, meaning that the clay-covered surface regions are less abundant. The higher coverage at pH 4 can be related to the higher positive charge of papain. Both small and larger saponite particles are deposited. At pH 8 the positive charge of papain is smaller and only able to attract "small" saponite particles.

The increase of the surface roughness from a "papain" surface to a "papain/saponite" surface is 0.88 nm (pH 4) and 0.64 nm (pH 8). This mainly reflects partial coverage of clay particles. There are significant differences between the $(PA/Sa)_1$ and PD-$(Sa/PA)_1$ sytems. The topography of PD-$(Sa/PA)_1$ in Figure 11c is very similar those of the fuzzy-assembled (PD/Sa) films of van Duffel et al.[18] In contrast to the $(PA/Sa)_1$ films, the height histogram of PD-$(Sa/PA)_1$ in Figure 11c is diffuse and apparently multimodal, which means that there is no specific height population that would characterize a relatively uniform distribution of clay particles on the surface. Particles with thicknesses of 13 nm up to 25 nm are present, indicating significant aggregation of saponite sheets. It is also remarkable that the substrate is practically fully covered by these aggregates. As a consequence, the average height of the PD-$(Sa/PA)_1$ bilayer and its roughness are considerably larger than those of the protein/Sa films.

Discussion

LbL is an effective and general procedure for the assembly of protein/clay films.[33,34,37] This is confirmed in the present investigation. UV−Vis, ATR-FTIR, and XRD experiments of the present study demonstrate the possibility of direct self-assembly of proteins and clay sheets on various substrates with and without a first polyelectrolyte layer. The as-compiled biofilms are stable and uniform, and their average thickness increases linearly with the dipping cycles up to at least 15 protein/clay bilayers. The fact that polyelectrolytes can be omitted makes the film deposition simpler (there are only two components). The detailed spectroscopic measurements allow us to discuss the mechanism of film formation and the structure of the protein and saponite layers in the mono- and multilayered films.

Driving Force for Formation of Direct Protein/Clay Self-Assembly. Electrostatic interactions seem to be dominant for the layer-by-layer build-up of our protein/clay systems for several resaons. First, the charge-compensating anions of protamine (SO_4^{2-}) and papain (phosphate) are completely missing in the biofilms. They are replaced by the negatively charged saponite sheets. This means that an ion exchange reaction takes place:

$$Na^+(H_2O)_n\text{−saponite} + \text{protein−anion} \rightarrow \text{protein−saponite} + Na^+(H_2O)_n + \text{anions} \quad (4)$$

The Na^+ ions and anions are washed away. Ion exchange is thermodynamically an equilibrium reaction. In the case of the protein under investigation, this equilibrium is strongly shifted to the right in eq 4 (unpublished results). It also means that ionic strength is an important parameter, but we have not investigated it in the present study. Second, the amount of saponite and thus the negative charges in the saponite layer is proportional with the positive charge density of proteins (and PD). The latter follows the order PD ≫ PR > LZ > PA (pH 4) > PA (pH 8). The amount of saponite in each layer, as measured by ATR-FTIR, decreases in the same order. Each layer contains excess charge, that is, more than needed to compensate the opposite charge of the previous layer according to eq 4. This is the basis for the construction of multilayers.

Electrostatic attraction between the protein and clay is not the only type of interaction. Kotov[53] has discussed two additional types of interactions: (i) Transformations in the ionic atmosphere (in our case) of the positively charged proteins and negatively charged saponite sheets. For the proteins, it is the replacement of anions by saponite sheets; for saponite, it is the replacement of Na^+ by proteins. (ii) These changes in ionic atmosphere are accompanied by changes in hydration (indeed, we found no detectable amounts of water in the films). These interactions are significant in our films too; however, it remains a challenge to quantify them.

Structure of Multilayered LbL Bionanofilms: *1. AFM/Glass Substrate*. When the proteins are directly deposited on glass, they form a monolayer. The thickness of this layer is 3 nm, corresponding roughly with the diameter of the proteins under investigation (Figure 11). When saponite sheets are deposited on this protein layer, they preferentially adsorb on the positively charged arrays of protein molecules. Deposition on the glass surface is less likely, because the latter is negatively charged and compensated by the positive charge of the proteins. The result is an increase in the surface roughness (see Table 3). This increase corresponds more or less to the thickness of the saponite sheet (0.96 nm). When this preferential adsorption of saponite sheets and protein molecules continues with construction of multilayers, the surface roughness will increase with the number of layers, as is indeed observed (Table 3). If the glass substrate is first covered with PD, the density of positive charges is so high that the saponite sheets aggregate into an assembly of particles on top of the PD layer, forming a thick rough layer of 15−25 nm (PD + Sa + PA) (Figure 11). PD is therefore not suited to prepare smooth films, the reason being the high positive charge density, in combination with the high molecular weight.

2. UV/Quartz Substrate. In Table 1 the average surface area/protein is given as deduced from the increase of the 194 nm band with the number of layers. This area is in all cases larger than the "theoretical" area calculated for a hexagonally close packed two-dimensional array of protein spheres. Thus the surface coverage is near or somewhat less than 100%, in agreement with the AFM observations for films on glass. The exception is the first layer on PD. There, the average surface area per protein molecule is 4−5 times smaller than the theoretical value. This is indicative of three-dimensional aggregation/ordering of protein molecules on top of the aggregates of saponite sheets. We can conclude that there is qualitative agreement between the results of the AFM measurements of the films on glass and the UV measurements of the films on quartz.

3. ATR/ZnSe Substrate. Mono- and multilayered films deposited on ZnSe can be used for ATR-FTIR investigation of the protein layers and the saponite layers separately. The average increase in the intensity of the amide I band and that of the Si−O stretching vibration have been used for that purpose. The increase in the amide I band per deposited protein layer is 0.03 au for LZ and PR, meaning that the same amount of peptide bonds is deposited in one layer of LZ and PR. For PA the amide I band increase is pH-dependent: 0.025 at pH 8 and 0.05 at pH4. Thus twice as much PA is deposited in one layer at pH 4 as at pH 8. This has to do with the positive charge on this protein, which is higher at pH 4 than at pH 8. It also confirms that PA at pH 8 is covered with a submonolayer of saponite sheets. The increase of the intensity of the 1000 cm^{-1} Si−O stretch of saponite follows the sequence PR > LZ > PA (pH 4) > PA (pH 8). This is also the sequence of decrease in protein charge per molecule. Thus, PR with the highest positive charge per molecule attracts more saponite layers (=more negative charges) than LZ and PA, again confirming the importance of electrostatic attraction of positively charged species in the film formation process. In a previous publication[43] we have shown that the intensity of the Si−O band for a monolayer of single saponite sheets of 1 nm thickness is around 0.1 au on a ZnSe crystal. This means that the average thickness of the saponite layer is that of a stack of 3 saponite sheets in the case of PR, 2 for LZ, and 2.5 for PA deposited at pH 4. Qualitative support for this is found in the AFM pictures. They show areas with thicknesses up to 5−7 nm, corresponding to one layer of proteins of 3 nm thickness and 2−3 saponite sheets on top. In conclusion, the "average" layer of saponite sheets in our LbL films is one that consists of single saponite sheets and particles of 2 or 3 saponite sheets.

TABLE 4: Measured Quantities and Derived Parameters Used for the Model Calculation[a]

sample	A	$A - A_{Sa}$	α	Θ (nm^{-2})	Ω (nm^2)
1st bilayer of PD-(Sa/PA), pH 8	0.114	0.108	0.108	0.378	2.6
2nd−15th bilayers of PD-(Sa/PA), pH 8	0.495	0.302	0.022	0.076	13.1
1st bilayer of PD-(Sa/PA), pH 4	0.112	0.106	0.106	0.372	2.7
2nd−15th bilayers of PD-(Sa/PA), pH 4	0.322	0.167	0.012	0.041	24.2
$(PA/Sa)_{15}$, pH 8	0.394	0.312	0.021	0.073	13.7
$(PA/Sa)_{15}$, pH 4	0.273	0.216	0.014	0.050	19.9
$(LZ/Sa)_{15}$	0.370	0.321	0.021	0.059	17.0
$(PR/Sa)_{15}$	0.359	0.233	0.016	0.145	6.9

[a] A, $A - A_{Sa}$, and α are measured quantities; Θ and Ω are derived parameters.

General Picture of Protein/Clay Multilayer Assembly. The general picture that emereges is as follows:

(1) $(Protein/Sa)_n$ films are quite regular and smooth. The film construction starts with a monolayer of protein molecules or less than a monolayer of protein molecules on the substrate. The coverage depends on the negative charge density of the substrate, the charge of protein, and possibly other factors, but we did not investigate this issue systematically. The subsequent layer of saponite sheets is, on average, 2−3 sheets thick, depending on the charge of the protein. This sequence is repeated very regularly up to 15 bilayers.

(2) When the construction of the layer is started with a PD layer, there is a high positive charge density on which saponite particles, several sheets thick, are deposited. The result is a thick (20−30 nm) rough bilayer. On this relatively thick layer, multilayers of saponite/protein bilayers are formed as described in the previous paragraph.

The regular sequence of protein and saponite layers is confirmed by our XRD measurements, showing typical first- and second-order d_{001} reflections, characteristic of monomolecular layers of proteins sandwiched between layers of saponite sheets. However, AFM topographic images and ATR-FTIR gave evidence for saponite particles composed of 2−3 single sheets. We do not know whether protein molecules can diffuse into the interlamellar space of the clay particles. Quite generally, we have no idea about the mobility of protein molecules and saponite sheets in the films or about the stability of the films as a function of time under various conditions. This is a point of more detailed investigation. Anyhow, the films are open or freely accessible to small molecules, as evidenced by the fast and reversible deuteration with D_2O. This is encouraging for development of sensing or other devices.

Conclusions

Mono-and multilayered clay/protein LbL films were successfully constructed on various supports with and without polyelectrolyte "sticking molecules". Deposition of the first bilayer on the polyelectrolyte-coated support afforded films with higher thickness and roughness, while in the absence of the polymer the films are more regular and smoother. Deposition of up to 15 bilayers proceeds in a regular fashion for protamine and lysozyme, while papain is partially lost (leached out or chemi-

cally degraded) from the biofilms when the film is dipped in the clay dispersion. Deuteration of protamine with D_2O is complete in 2 h, and deuteration is almost complete in the case of lysozyme and papain. Deuteration is also reversible in all cases, which is indirect proof that the structure of the proteins is conserved in the films to a large extent. The collection of results from complementary characterization techniques (UV−vis, ATR-FTIR, XRD, and AFM) provide detailed information on the layer-by-layer build-up of the multilayers. Especially, we must stress that it is worth monitoring the build-up after the deposition of each layer, and not only after deposition of bilayers, as is usually the case in the literature. This is because careful monitoring may reveal unexpected processes (degradation, desorption, structural changes, etc.) occurring upon progressive multilayer formation.

LbL assembly offers advantages over other techniques such as Langmuir−Blodgett (LB) or spin coating. (1) LB deposition has limited applicability as it requires amphiphilic molecules. (2) Spin coating requires large amounts of solutions, and the film thickness and homogeneity are less controllable. (3) Covering objects of complex geometry/shape is possible by LbL, but spin coating and LB afford films only on flat or slightly bent surfaces. Thus, coating of tools or equipments (e.g., in medicine and surgery) with nanostructured, functional biofilms is promising. Functions may include antibacterial protection (lysozyme), proteolytic surface (papain), or in situ control of biochemical processes (protamine).

Construction of nanostructured layers is the basis for the development of biosensors and biocatalysts.[19−21,54−56] Detailed characterization of the enzyme activity and substrate accessibility in the present protein/clay multilayers and comparison with those of conventional protein/polyelectrolyte films are the first steps to reach this objective.

Acknowledgment. This research was financially supported by the Intergovernmental Science and Technology Cooperation between Flanders and Hungary (Projects BIL 04/ 32 and B-17/ 04) and by the IAP-VI and the Hungarian Scientific Research Fund OTKA (Project T/F 42715).

Appendix

Calculation of the Amount and Packing Density of Deposited Protein Molecules. An estimate of the protein coverage (packing density) and the adsorbed amounts of protein molecules in the different multilayers can be obtained in terms of the optical properties of protein solutions and $(protein/Sa)_n$ and $(PD/Sa)_n$ films. Table 4 shows the experimental data used and the results of the calculation procedure.

First, the individual contributions of the protein to the absorbance measured at 194 nm (A) is determined. Since the $(PD/Sa)_n$ films reflect the optical features of the clay particles only (note that PD is completely transparent even at this low wavelength), this aim can be reasonably accomplished by substracting the spectra of a $(PD/Sa)_n$ film (A_{Sa}) from those of the protein/clay films ($A - A_{Sa}$). Generally, the amount of clay in the films depends on the type of colloid acting as the "sticking material". So different assemblies of the same bilayer number do not have the same clay content and, consequently, the same absorption in the visible region, where the protein is transparent. Therefore, the $(PD/Sa)_n$ bilayer number needs to be chosen so that the spectrum fits well on that of the $(protein/Sa)_n$ assembly at $\lambda > 350$ nm as depicted in Figure 1. Next, the absorbance (α) is specified by the bilayer number to obtain the extinction of protein molecules deposited in one given dipping step as follows:

$$\alpha_1 = A - A_{Sa} \tag{A1}$$

for the first papain layer in PD-$(Sa/PA)_n$ films;

$$\alpha_{2-15} = \frac{(A - \alpha_1 - A_{Sa})}{14} \tag{A2}$$

for the 2nd−15th papain layers in PD-$(Sa/PA)_n$ films; and

$$\alpha = \frac{(A - A_{Sa})}{15} \tag{A3}$$

for all of the protein layers in $(PA/Sa)_n$, $(LZ/Sa)_n$, and $(PR/Sa)_n$ films. According to the Beer−Lambert law, the absorbance of one layer of protein molecules, sandwiched between two adjacent clay layers is given by

$$\alpha = \epsilon 2lc \tag{A4}$$

where l is the path length of the light beam passing through one protein monolayer of the film and c is the volume concentration of the protein in the monolayer. The factor 2 is involved because both sides of the support are covered by the ultrathin film. Therefore the light passes through a double number of layers. The specific extinction coefficients of immobilized proteins at 194 nm (ϵ) is assumed to be equal to those in aqueous solution. The latter were determined to be 36 740, 76 633, and 71 785 cm^2/g for papain, lysozyme, and protamine, respectively.

The concentration can be expressed by the mass (m) and volume of the adsorbed layer, the latter being equal to the product of layer thickness and surface area (S):

$$\alpha = \epsilon 2l\frac{m}{Sl} = 2\epsilon\frac{m}{S} \tag{A5}$$

With $m = nM$ (n = moles of the protein with molecular weight M) one obtains

$$\alpha = 2\epsilon M\frac{n}{S} \tag{A6}$$

With $N = nN_A$, the total number of molecules in the monolayer, we obtain the surface coverage Θ:

$$\Theta = \frac{N}{S} = \frac{N_A}{2\epsilon M}\alpha \tag{A7}$$

It is worth mentioning here that, for a given protein, the surface concentration depends solely on the absorbance α, which is a readily available quantity. Substitution gives a simplified equation for the surface (layer) coverage of protein:

$$\Theta\ (nm^{-2}) = 3.563\ (nm^{-2})\alpha \tag{A8}$$

Finally, the inverse of Θ provides the average surface area of one protein molecule:

$$\Omega = \frac{S}{N} = \frac{1}{\Theta} \tag{A9}$$

References and Notes

(1) Hammond, P. T. *Curr. Opin. Colloid Interface Sci.* **2000**, *4*, 430.
(2) Decher, G. *Science* **1997**, *277*, 1232.
(3) Caruso, F. In *Colloids and Colloid Assemblies*; Caruso, F., Ed.; Wiley: New York, 2004; p 246.
(4) Jiang, M.; Wang, E.; Wei, G.; Xu, L.; Kang, Z.; Lian, S. *J. Colloid Interface Sci.* **2004**, *275*, 596.

(5) Kotov, N. A.; Dékány, I.; Fendler, J. H. *J. Phys. Chem.* **1995**, *99*, 13065.
(6) Kun, R.; Balázs, M.; Dékány, I. *Colloids Surf., A* **2005**, *265*, 155.
(7) Szabó, T.; Szeri, A.; Dékány, I. *Carbon* **2005**, *43*, 87.
(8) Chirea, M.; García-Morales, V.; Manzanares, J. A.; Pereira, C.; Gulaboski, R.; Silva, F. *J. Phys. Chem. B* **2005**, *109*, 21808.
(9) van Duffel, B.; Schoonheydt, R. A.; Grim, C. P. M.; DeSchryver, F. C. *Langmuir* **1999**, *15*, 7520.
(10) Kleinfeld, E. R.; Ferguson, G. S. *Science* **1994**, *265*, 370.
(11) Kotov, N. A.; Haraszti, T.; Turi, L.; Zavala, G.; Geer, R. E.; Dékány, I.; Fendler, J. H. *J. Am. Chem. Soc.* **1997**, *119*, 6821.
(12) Glinel, K.; Laschewsky, A.; Jonas, A. M. *Macromolecules* **2001**, *34*, 5267.
(13) Fan, X.; Park, M.-K.; Xia, C.; Advincula, R. *J. Mater. Res.* **2002**, *17*, 1622.
(14) Lagaly, G.; Ogawa, M.; Dékány, I. In *Handbook of Clay Science*; Bergaya, F., Theng, B. K. G., Lagaly, G., Eds.; Elsevier: Amsterdam, 2006; p 309.
(15) Kleinfeld, E. R.; Ferguson, G. S. *Chem. Mater.* **1995**, *7*, 2327.
(16) Mamedov, A.; Ostrander, J.; Aliev, F.; Kotov, N. A. *Langmuir* **2000**, *16*, 3941.
(17) Podsiadlo, P.; Paternel, S.; Rouillard, J. M.; Zhang, Z. F.; Lee, J.; Lee, J. W.; Gulari, L.; Kotov, N. A. *Langmuir* **2005**, *21*, 11915.
(18) van Duffel, B.; Verbiest, T.; van Elshocht, S.; Persoons, A.; De Schryver, F. C.; Schoonheydt, R. A. *Langmuir* **2001**, *17*, 1243.
(19) Zhou, Y.; Li, Z.; Hu, N.; Zeng, Y.; Rusling, J. F. *Langmuir* **2002**, *18*, 8573.
(20) Liu, H. Y.; Rusling, J. F.; Hu, N. F. *Langmuir* **2004**, *20*, 10700.
(21) Hiller, S.; Leporatti, S.; Schnackel, A.; Typlt, E.; Donath, E. *Biomacromolecules* **2004**, *5*, 1580.
(22) Papp, S.; Dékány, I. *Colloid Polym. Sci.* **2003**, *281*, 727.
(23) Bourlinos, A. B.; Karakassides, M. A.; Simopoulos, A.; Petridis, D. *Chem. Mater.* **2000**, *12*, 2640−2645.
(24) Bourlinos, A. B.; Jiang, D. D.; Giannelis, E. P. *Chem. Mater.* **2004**, *16*, 2404.
(25) Schoonheydt, R. A. *Clays Clay Miner.* **2002**, *50*, 411.
(26) Bakandritsos, A.; Steriotis, T.; Petridis, D. *Chem. Mater.* **2004**, *16*, 1551.
(27) Sanjay, G.; Sugunan, S. *Food Chem.* **2006**, *94*, 573.
(28) Carrado, K. A.; Macha, S. M.; Tiede, D. M. *Chem. Mater.* **2004**, *16*, 2559.
(29) Szilágyi, I.; Horváth, L.; Labádi, I. Hernádi, K.; Pálinkó, I.; Kiss, T. *Cent. Eur. J. Chem.* **2006**, *4*, 118.
(30) Szilágyi, I.; Labádi, I.; Hernádi, K.; Pálinkó, I.; Fekete, I.; Korecz, L.; Rockenbauer, A.; Kiss, T. *New J. Chem.* **2005**, *29*, 740.
(31) Theng, B. K. G. *The Chemistry of Clay Organic Reactions*; Adam Hilger: London, 1974.
(32) Quiquampoix, H.; Staunton, S.; Baron, M. H.; Ratcliffe, R. G. *Colloids Surf., A* **1993**, *75*, 85.
(33) Decher, G.; Lehr, B.; Lowack, K.; Lvov, Y.; Schmitt, J. *Biosens. Bioelectron.* **1994**, *9*, 677.
(34) Lvov, Y.; Ariga, K.; Ichinose, I.; Kunitake, T. *J. Am. Chem. Soc.* **1995**, *117*, 6117.
(35) Finley, J. W.; Stanley, W. L.; Watters, G. G. *Process Biochem.* **1979**, *14*, 12.
(36) Stepek, G.; Buttle, D. J.; Duce, I. R.; Lowe, A.; Behnke, J. M. *Parasitology* **2005**, *130*, 203.
(37) Qi, Z. M.; Honma, I.; Zhou, H. *Adv. Funct. Mater.* **2006**, *16*, 377.
(38) http://www.sci.sdsu.edu/TFrey/Bio750/UV-VisSpectroscopy.html.
(39) Kaul, P.; Sathish, H. A.; Prakash, V. *Nahrung* **2002**, *46*, 2.
(40) Harpaz, Y.; Gerstein, M.; Chothia, C. *Structure* **1994**, *2*, 641.
(41) Rubtsov, I. V.; Wang, J.; Hochstrasser, R. M. *J. Phys. Chem. A* **2003**, *107*, 3384.
(42) Chung, H. S.; Tokmakoff, A. *J. Phys. Chem. B* **2006**, *110*, 2888.
(43) Ras, R. H. A.; Németh, J.; Johnston, C. T.; DiMasi, E.; Dékány, I.; Schoonheydt, R. A. *Phys. Chem. Chem. Phys.* **2004**, *6*, 4174.
(44) Nakamoto, K. *Infrared and Raman spectra of inorganic and coordination compounds*, 5th ed.; Wiley: New York, 1997.
(45) Ottensmeyer, F. P.; Whiting, R. F.; Korn, A. P. *Proc. Natl. Acad. Sci. U.S.A.* **1975**, *72*, 4953.
(46) Dong, A. C.; Prestrelski, S. J.; Allison, S. D.; Carpenter, J. F. *J. Pharm. Sci.* **1995**, *84*, 415.
(47) Petrosyan, A. M. *Vib. Spectrosc.* **2006**, *41*, 97.
(48) Braiman, M. S.; Briercheck, D. M.; Kriger, K. M. *J. Phys. Chem. B* **1999**, *103*, 4744.
(49) Green, R. J.; Hopkinson, I.; Jones, R. A. L. *Langmuir* **1999**, *15*, 5102.
(50) Perutz, M.; Muirhead, H.; Cox, J.; Goaman, L.; Mathews, L.; Mcgandy, E.; Webb, L. *Nature* **1968**, *219*, 29.
(51) Fan, X.; Locklin, J.; Youk, J. H.; Blanton, W.; Xia, C.; Advincula, R. *Chem. Mater.* **2002**, *14*, 2184.
(52) Kim, D. T.; Blanch, H. W.; Radke, C. J. *Langmuir* **2002**, *18*, 5841.
(53) Kotov, N. A. *Nanostruct. Mater.* **1999**, *12*, 789.
(54) Mousty, C. *Appl. Clay Sci.* **2004**, *27*, 159.
(55) Tyner, K. M.; Roberson, M. S.; Berghorn, K. A.; Li, L.; Gilmour, R. F., Jr.; Batt, C. A.; Giannelis, E. P. *J. Controlled Release* **2004**, *100*, 399.
(56) Li, Z.; Hu, N. *J. Electroanal. Chem.* **2003**, *558*, 155.